6-1-2022

Angiogenin released from ABCB5+ stromal precursors improves healing of diabetic wounds by promoting angiogenesis

Karmveer Singh

Pallab Maity

Albert Kallon Koroma

Abhijit Basu

Rajeev Kumar Pandey

See next page for additional authors

10.1016/j.jid.2021.10.026
Singh, K., Maity, P., Koroma, A. K., Basu, A., Pandey, R. K., Vander Beken, S., ... & Scharffetter-Kochanek, K. (2022).
Angiogenin Released from ABCB5+ Stromal Precursors Improves Healing of Diabetic Wounds by Promoting
Angiogenesis. Journal of Investigative Dermatology, 142(6), p. 1725-1736. https://doi.org/10.1016/
j.jid.2021.10.026

Authors

Karmveer Singh, Pallab Maity, Albert Kallon Koroma, Abhijit Basu, Rajeev Kumar Pandey, Seppe Vander Beken, Philipp Haas, Linda Krug, Adelheid Hainzl, Anca Sindrilaru, Christiane Pfeiffer, Meinhard Wlaschek, Natasha Y. Frank, Markus H. Frank, Christoph Ganss, András Bánvölgyi, Norbert Wikonkál, Sabine Eming, Irena Pastar, Marjana Tomic-Canic, Mark A. Kluth, and Karin Scharffetter-Kochanek

Angiogenin Released from ABCB5+ Stromal Precursors Improves Healing of Diabetic Wounds by Promoting Angiogenesis

*JID*Open

Karmveer Singh[1,15], Pallab Maity[1,15], Albert Kallon Koroma[1], Abhijit Basu[1], Rajeev Kumar Pandey[1,2], Seppe Vander Beken[1,3], Philipp Haas[1], Linda Krug[1], Adelheid Hainzl[1], Anca Sindrilaru[1], Christiane Pfeiffer[1], Meinhard Wlaschek[1], Natasha Y. Frank[4,5,6], Markus H. Frank[4,7,8,9], Christoph Ganss[10,11], András Bánvölgyi[12], Norbert Wikonkál[12], Sabine Eming[13], Irena Pastar[14], Marjana Tomic-Canic[14], Mark A. Kluth[10,11,16] and Karin Scharffetter-Kochanek[1,16]

Severe angiopathy is a major driver for diabetes-associated secondary complications. Knowledge on the underlying mechanisms essential for advanced therapies to attenuate these pathologies is limited. Injection of ABCB5+ stromal precursors at the edge of nonhealing diabetic wounds in a murine *db/db* model, closely mirroring human type 2 diabetes, profoundly accelerates wound closure. Strikingly, enhanced angiogenesis was substantially enforced by the release of the ribonuclease angiogenin from ABCB5+ stromal precursors. This compensates for the profoundly reduced angiogenin expression in nontreated murine chronic diabetic wounds. Silencing of angiogenin in ABCB5+ stromal precursors before injection significantly reduced angiogenesis and delayed wound closure in diabetic *db/db* mice, implying an unprecedented key role for angiogenin in tissue regeneration in diabetes. These data hold significant promise for further refining stromal precursors—based therapies of nonhealing diabetic foot ulcers and other pathologies with impaired angiogenesis.

[1]Department of Dermatology and Allergic Diseases, Ulm University, Ulm, Germany; [2]Department of Oncology, Johns Hopkins School of Medicine, Baltimore, Maryland, USA; [3]Bredent medical GmbH & Co KG, Senden, Germany; [4]Transplant Research Program, Boston Children's Hospital, Boston, Massachusetts, USA; [5]Department of Medicine, VA Boston Healthcare System, Boston, Massachusetts, USA; [6]Division of Genetics, Brigham and Women's Hospital, Harvard Medical School, Boston, Massachusetts, USA; [7]Harvard Skin Disease Research Center, Department of Dermatology, Brigham and Women's Hospital, Harvard Medical School, Boston, Massachusetts, USA; [8]Harvard Stem Cell Institute, Harvard University, Cambridge, Massachusetts, USA; [9]School of Medical and Health Sciences, Edith Cowan University, Perth, Australia; [10]TICEBA GmbH, Heidelberg, Germany; [11]RHEACELL GmbH & Co KG, Heidelberg, Germany; [12]Department of Dermatology, Venereology and Dermatooncology, Faculty of Medicine, Semmelweis University, Budapest, Hungary; [13]Department of Dermatology and Venereology, University of Cologne, Cologne, Germany; and [14]Wound Healing and Regenerative Medicine Research Program, Dr Phillip Frost Department of Dermatology and Cutaneous Surgery, Miller School of Medicine, University of Miami, Miami, Florida, USA

[15]These authors contributed equally to this work.

[16]These authors contributed equally as senior authors.

Correspondence: Karin Scharffetter-Kochanek, Department of Dermatology and Allergic Diseases, Ulm University, Albert-Einstein-Allee 23, 89081 Ulm, Germany. E-mail: karin.scharffetter-kochanek@uniklinik-ulm.de

Abbreviations: Akt, protein kinase B; ANG, angiogenin; HUVEC, human umbilical vein endothelial cell; siRNA, small interfering RNA; SP, stromal precursor; WT, wild type

Received 26 November 2020; revised 5 October 2021; accepted 14 October 2021; accepted manuscript published online 20 Novermber 2021; corrected proof published online 15 January 2022

INTRODUCTION

Diabetes mellitus is an urgent global health problem imposing a significant socioeconomic burden on societies. Around 600 million people are predicted to suffer from diabetes by 2045 (Aldworth et al., 2017), and in consequence, secondary complications such as nonhealing wounds will profoundly increase. The most important among them are vascular pathologies, including microangiopathy and macroangiopathy. In fact, the vast majority of patients undergoing nontraumatic lower-limb amputations have diabetes (Armstrong et al., 2020). Despite major efforts (Okonkwo et al., 2020; Tahergorabi and Khazaei, 2012), the mechanisms of vasculopathies and reduced angiogenesis in diabetes are still not sufficiently understood. In consequence, there is an outstanding interest to (i) get better insight into how angiogenesis is suppressed and (ii) to further advance therapies to improve angiogenesis in chronic wounds in diabetes. Of particular clinical relevance are stem cell–based therapies that will be cost saving in long term in chronic wounds and other conditions (Augustin and Vanscheidt, 2012; Soria-Juan et al., 2019; Thavorn et al., 2020).

Stromal precursors (SPs) in their endogenous niche in the skin are largely unexplored under diabetic conditions. The beneficial effects of SP therapies, although incompletely understood for diabetes, are primarily due to paracrine signals in wound models (Davey et al., 2014; Jiang et al., 2013; Qi et al., 2014; Vander Beken et al., 2019). In this study, we are interested in finding whether local administration of SPs at the wound site enhances angiogenesis and restores delayed wound healing in diabetic wounds.

A major obstacle still impeding the successful implementation of SP-based therapies in clinical routine is the lack of a cell-surface marker that reliably allows to isolate SPs from the skin to further enrich, expand, and reproducibly test them for their paracrine efficiency and potency. Previously, we identified a cell population in the dermis expressing the adenosine triphosphate-binding cassette subfamily B member 5 (ABCB5) in addition to well-established SP cell markers (Vander Beken et al., 2019). These ABCB5$^+$ SPs can suppress effector T cells while stimulating regulatory T cells in vitro and in vivo (Schatton et al., 2015). In addition, ABCB5$^+$ SPs suppress the unrestrained activation of proinflammatory M1 macrophages in a murine iron-overload model (Vander Beken et al., 2019). Employing antibodies against ABCB5, it is possible to reliably isolate ABCB5$^+$ SPs under Good Manufacturing Practice standards to a homogeneous population, which even after in vitro expansion partly maintains their stemness, maintains mesenchymal expression profile, and meets stringent quality criteria (Tappenbeck et al., 2019; Vander Beken et al., 2019).

RESULTS

Diabetic conditions suppress angiogenesis and rewire the global transcriptome of endothelial cells

To assess the influence of obesity-induced diabetes on angiogenesis, we first performed in vitro tube formation assay indicative of angiogenesis. For this purpose, human umbilical vein endothelial cells (HUVECs) were cocultured with fibroblasts from either wild-type (WT) or db/db mice. The db/db mice closely mimic metabolic changes in human type 2 diabetes (Chen et al., 1996). Blood vessel (tube) formation was severely suppressed in the presence of db/db mouse fibroblasts as opposed to that of WT fibroblasts (Figure 1a and b). These results clearly show detrimental consequences of db/db stromal fibroblasts on endothelial cell function.

To further identify the underlying mechanisms that impair endothelial cell function, we cocultured HUVECs with fibroblasts from either WT or db/db mice for 5 days, followed by transcriptomic analysis of FACS-sorted HUVECs. We observed marked alterations in the global transcriptome of HUVECs after coculture with db/db fibroblasts as opposed to that with WT fibroblasts (Figure 1c). After coculture with db/db fibroblasts, we observed upregulation of proinflammatory cytokines (Il-6 and Il1β), matrix-degrading enzymes (Mmp1, Mmp7, Mmp10, and Mmp19), and tumor angiogenesis suppressor (Tp73) genes as well as genes associated with DNA damage response (Rad51, Rad9b, and Xrcc2), senescence (Cdkn2a or p16), and apoptosis (Faslg) (Figure 1c). By contrast, genes regulating endothelial adhesion and migration, including Vcam1, Kif26a, and Itgb4, were downregulated in HUVECs cocultured with db/db fibroblasts as opposed to that cocultured with WT fibroblasts (Figure 1c).

Furthermore, pathway enrichment analysis revealed overrepresentation of cytokine signaling, apoptosis, IL-1 signaling, collagen degradation, and DNA repair pathway in HUVECs cocultured with db/db fibroblasts compared with that cocultured with WT fibroblasts (Figure 1d). The pathways associated with Notch signaling, protein kinase B (Akt) signaling, integrin cell-surface interactions, and IL-10 signaling were underrepresented in HUVECs cocultured with db/db fibroblasts compared with that cocultured with WT fibroblasts (Figure 1e). Consistent with these findings, HUVEC numbers markedly declined after 5 days of coculture with db/db stromal fibroblasts as opposed to that with WT fibroblasts (Supplementary Figure S1a). In aggregate, these findings indicate that adverse signaling of diabetic fibroblasts severely impairs endothelial cell homeostasis and promotes angiogenesis-suppressing and angiopathy-associated gene programs.

Vascular network and numbers of SP diminish in diabetes

Next, we examined angiogenesis in the skin of adult mice with diabetes. Severely reduced numbers of CD31$^+$ vessels were observed in the skin of mice with diabetes as opposed to the skin of WT mice (Figure 2a). We hypothesized that local signals originating from SP cells are essential for endothelial function and homeostasis. Therefore, we explored the endogenous stromal niche for distinct SP subsets to understand whether diabetes may affect the endogenous stromal niche. Immunostaining of skin sections was performed with antibodies against ABCB5 that specifically identify a subset of SPs (Vander Beken et al., 2019). Interestingly, a severe reduction in the number of ABCB5$^+$ SPs was found in the dermis of db/db mice as opposed to that of WT mice (Figure 2b). We also observed a marked decrease in ABCB5$^+$ SP numbers in close vicinity to blood vessels in the skin from mice with diabetes (Supplementary Figure S1b). The number of ABCB5$^+$ SPs was also severely reduced during tissue repair in mice with diabetes compared with higher numbers in WT (Supplementary Figure S1c). We also observed a marked reduction in other SPs, including PDGFRβ$^+$, Nestin$^+$, and CD34$^+$ cells (Koliaraki et al., 2020), in db/db mouse skin compared with that in WT mouse skin (Supplementary Figure S2a). This may imply that metabolic changes in diabetes profoundly affect many types of SP cells in their endogenous niche.

Furthermore, our data unveiled a transcriptomic profile fundamentally different in endothelial cells derived from db/db mice as opposed to that from WT mice (Figure 2c). Genes linked to Notch signaling (Hey2), VEGF signaling (Vegfa and Vegfb, Vegfc, Flt1, Flt4, and Kdr), IGF-1–Akt signaling (Ip6k3), and ribosomal biogenesis (Rpl7a and Cars1) and genes encoding for the actin-organizing protein Klhl1 and the negative regulator of autophagy Tmem208 were suppressed in either arteries or veins (Figure 2c). By contrast, genes linked to DNA double-strand breaks (Aunip), the gene encoding RPAP3 (Rpap3), and the G protein receptor coding gene Gpr165 were upregulated in blood vessels from mice with diabetes as opposed to those from WT mice (Figure 2c). The principal component analysis plot revealed a close clustering of diabetic arteries and veins compared with a broader distribution of WT markers, indicating that both types of vessels undergo marked remodeling and transcriptional alteration under diabetic environment (Supplementary Figure S2b). Similar to pathway enrichment analysis of the coculture experiments with endothelial cells and db/db fibroblasts (Figure 1d and e), the signature of endothelial cells from arteries and veins of db/db mice—representing the diabetic microenvironment in vivo—also revealed overrepresentation of cytokine signaling, apoptosis, degradation
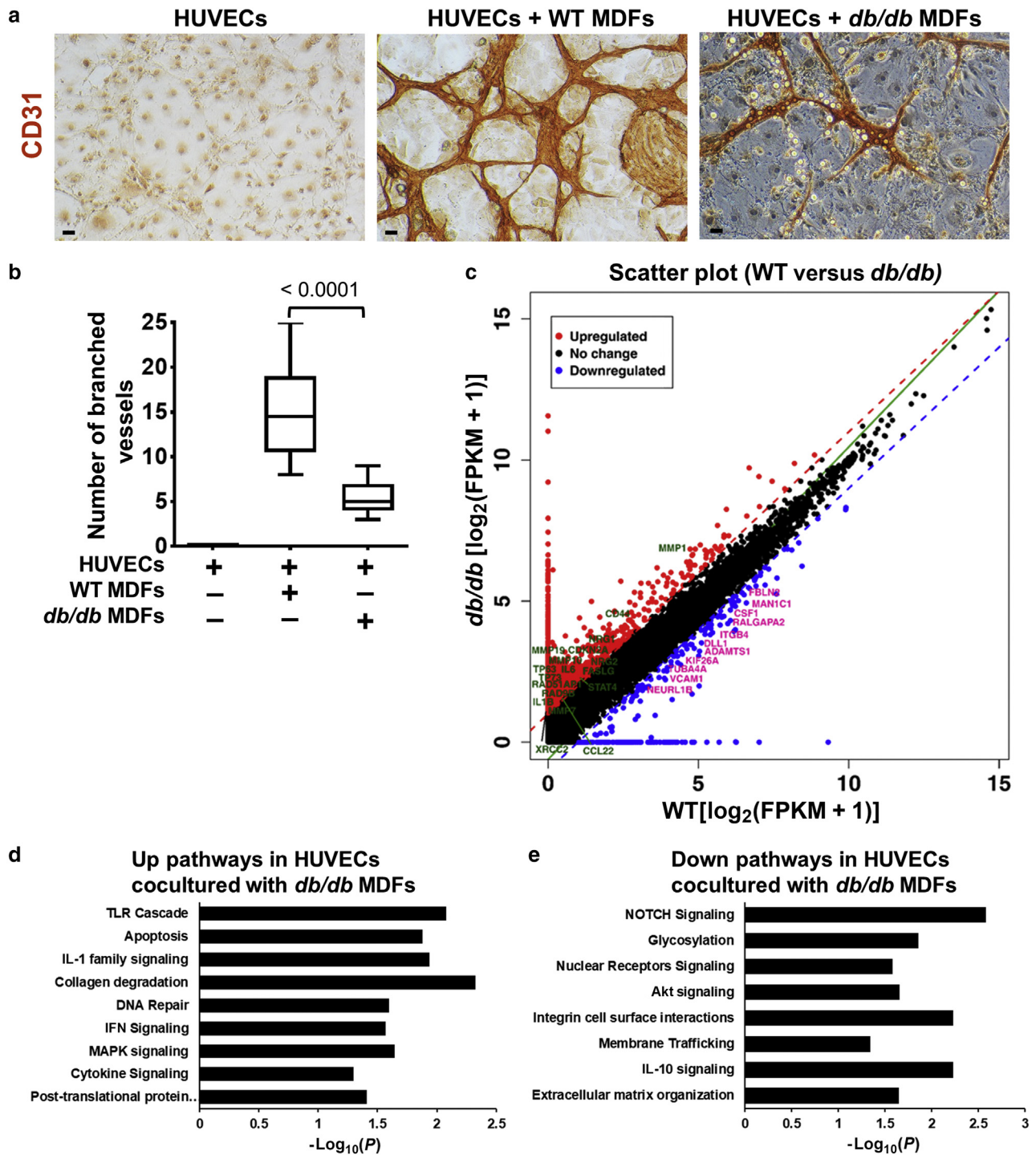
Figure 1. Diabetic stroma suppresses angiogenesis and leads to profound transcriptomic alterations in endothelial cells. (**a**) In vitro angiogenesis from cocultures of endothelial cells (HUVECs) with WT mouse fibroblasts (WT MDFs, middle panel) or *db/db* mouse fibroblasts (*db/db* MDFs, right panel). HUVECs cultured alone (left panel) served as a negative control. Bar = 50 μM. (**b**) Quantification of branched vessels in the angiogenesis assay at 14 days of coculture. Statistical analysis was performed using one-way ANOVA; values are represented as mean ± SEM, n = 3. (**c**) Scatter plot showing differentially regulated genes and (**d**) pathway enrichment analysis showing the key significantly enriched signaling pathways, which are upregulated or (**e**) downregulated in HUVECs after 5 days of coculture with db/db mouse fibroblasts compared with that of WT mouse fibroblasts. Akt, protein kinase B; FPKM, Fragments Per Kilobase of transcript per Million mapped reads; HUVEC, human umbilical vein endothelial cell; MDF, murine dermal fibroblast; SP, stromal precursor; TLR, toll-like receptor; WT, wild type.

of extracellular matrix, IFN signaling, and DNA damage pathways (Figure 2d and Supplementary Figure S2c). Of note, the pathways associated with VEGF signaling, insulin IGF-1/ Akt signaling, and ribosomal RNA processing were underrepresented in blood vessels from mice with diabetes compared with those from WT mice (Figure 2e and Supplementary Figure S2d). These data imply that microenvironmental cues originating in part from the stromal
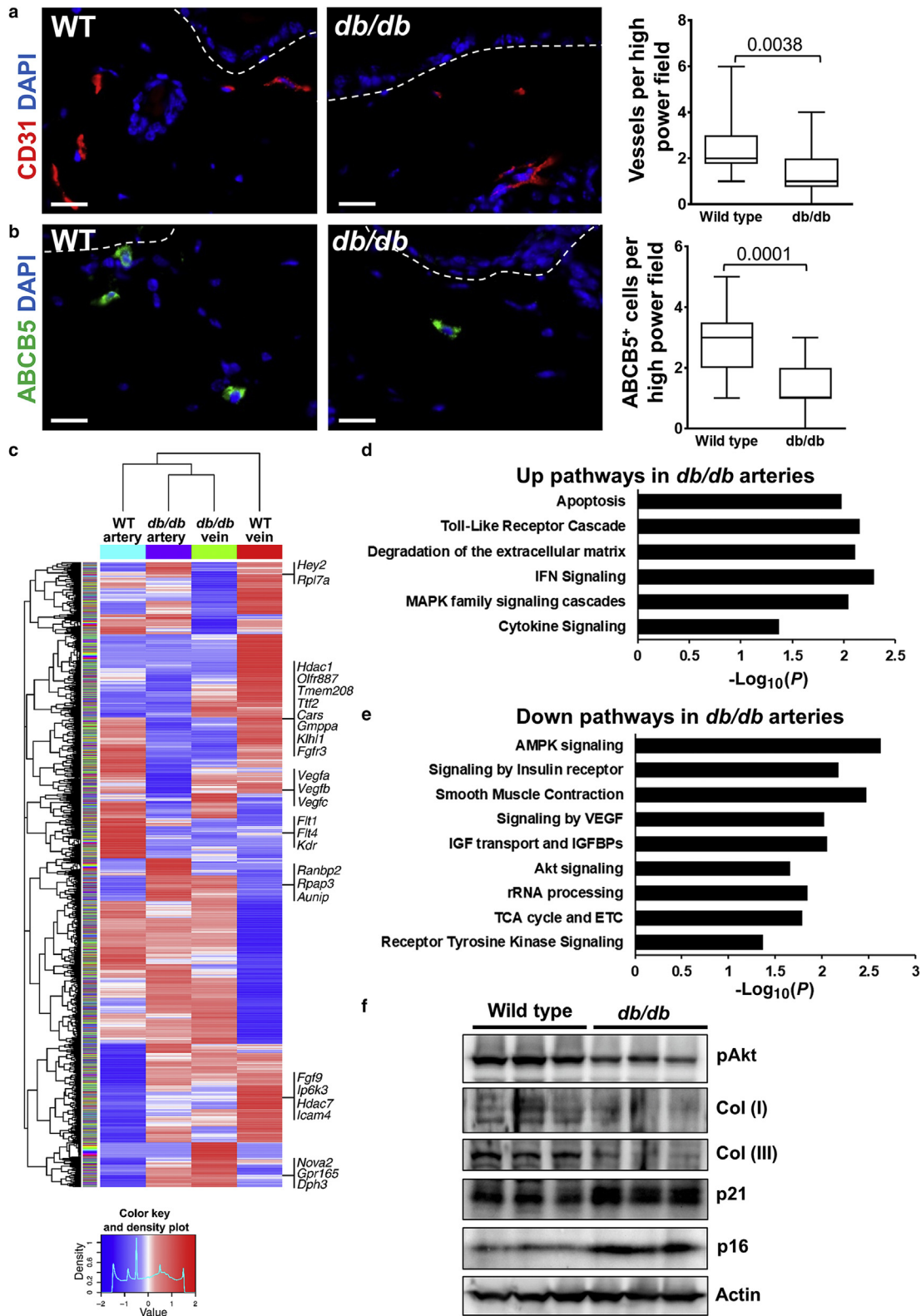
Figure 2. Diabetes severely affects the vascular and stromal compartment. (**a**) Immunostaining and quantification of blood vessels marker CD31 (red) and (**b**) ABCB5^{+} (green) marking dermal SPs population in WT and *db/db* mouse skin. Bar = 20 μm. Statistical analysis was performed using unpaired *t*-test; values are represented as mean ± SEM, n = 3. (**c**) Heatmap shows the gene expression profile of arteries and veins isolated from WT and *db/db* mice. (**d**) Pathway enrichment analysis demonstrating the key significantly enriched signaling pathways, which are upregulated or (**e**) downregulated in *db/db* mice–derived arterial blood vessels compared with that in the WT. (**f**) Western blot analysis of indicated proteins from skin lysates of WT and *db/db* mice. This western blot is representative of three independent experiments. Quantification is shown in Supplementary Figure S3b. Akt, protein kinase B; AMPK, adenosine monophosphate-activated protein kinase; Col, collagen; ETC, electron transport chain; pAkt, phosphorylated protein kinase B; rRNA, ribosomal RNA; SP, stromal precursor; TCA, tricarboxylic acid; WT, wild type.

compartment in mice with diabetes impact endothelial cell signaling and function.

In this context, we observed markedly reduced collagen deposition in the dermis of mice with diabetes as opposed to that of WT mice (Figure 2f and Supplementary Figure S3a and b). Interestingly, enhanced expression of senescence markers p21 and p16 (Meyer et al., 2017; Ressler et al., 2006) was observed in the skin of *db/db* mice with diabetes aged 3 months as opposed to that of WT mice (Figure 2f and Supplementary Figure S3b). These data highlight that the dermal stromal compartment, as a part of the endogenous niche, is significantly affected in the skin of mice with diabetes and may disrupt the niche environment of SPs.

ABCB5$^+$ SPs enhance angiogenesis and accelerate wound healing in *db/db* mice

Previously, it was reported that wound healing is impaired in *db/db* mice (Chen et al., 1996; Xiao et al., 2016). On the basis of our observations that the stromal compartment, including the endogenous niche of SP cells, is profoundly affected in *db/db* mice and that SPs were reduced in numbers in the *db/db* skin, we next wished to explore whether an introduction of SP cells at the wound site may be beneficial for the wound-healing deficiency in mice with diabetes.

To exclude any engraftment or cell fusion effects, we purposely used an established xenotransplant model (Vander Beken et al., 2019) with local injection of human-derived ABCB5$^+$ SPs into the wounds of *db/db* mice. Intradermal injection of either PBS (vehicle) (100 μl), 1×10^6 human dermal fibroblasts (100 μl), or human skin–derived 1×10^6 ABCB5$^+$ SPs (100 μl) was performed at the wound edge in *db/db* mice with diabetes (Figure 3a).

Quantitative analysis of wound areas shows that administration of 1×10^6 ABCB5$^+$ SPs per wound substantially enhanced wound closure on days 3, 5, 7, and 10 (Figure 3b) as opposed to that in vehicle-treated mice with diabetes (compare the median of filled triangles [*db/db* mice with vehicle] with that of filled circles [*db/db* mice] with ABCB5$^+$ SPs). ABCB5$^+$ SPs-injected wounds showed better wound closure on days 5, 7, and 10 than fibroblasts-injected wounds (compare the median of filled rectangles [*db/db* mice with fibroblasts] with that of filled circles [*db/db* mice] with ABCB5$^+$ SPs) (Figure 3b). Injection of fibroblasts improved wound healing on day 7 when compared with that of PBS-injected wounds (compare the median of filled rectangles [*db/db* mice with fibroblasts] with that of filled triangles [*db/db* mice with vehicle]) (Figure 3b). These results suggest a therapeutic benefit of ABCB5$^+$ SPs for wounds in mice with diabetes.

Consistent with these findings, we observed smaller wound areas and marked matrix deposition (depicted by eosin-stained material) after ABCB5$^+$ SPs injection (Figure 3c). We next analyzed the newly formed vessels in wounds by immunostaining with antibodies against CD31, indicative of endothelial cells. Interestingly, injection of ABCB5$^+$ SPs significantly enhanced angiogenesis in *db/db* mice wounds compared with that in the vehicle (PBS)- and fibroblast-treated wounds (Figure 3d). These findings suggest that the beneficial role of ABCB5$^+$ SPs on diabetic wound therapy is at least in part due to enhanced angiogenesis.

Diabetic microenvironment abrogates angiogenin expression

Next, we set out to dissect the underlying mechanisms by which ABCB5$^+$ SPs accelerate wound healing and stimulate angiogenesis. We first analyzed the secretome of ABCB5$^+$ SPs to address the question of whether they release trophic or proangiogenic factors, which may enhance angiogenesis and, thus, improve impaired angiogenesis. Employing antibody arrays, we uncovered significant enrichment of the key proangiogenic factor angiogenin (ANG) in supernatants collected from ABCB5$^+$ SPs (Figure 4a). ANG is a secreted ribonuclease that plays a key role in stimulating angiogenesis (Cho et al., 2005). This 14.1-kDa monomeric protein constitutes the fifth member of the secreted ribonuclease family (Riordan, 2001). A strong expression of ANG in the antibody array was confirmed by western blot analysis of cell lysates from ABCB5$^+$ SPs compared with low ANG release from dermal fibroblasts (Figure 4b). In addition, MDC, MCP4, IGFBP3, TIMP2, and OPG were also induced in the supernatants of ABCB5$^+$ SPs (Figure 4a).

Because we were interested in the question of how suppressed angiogenesis could be restored in diabetic wounds, we selected ANG as an angiogenesis-stimulating factor to be further studied, although other upregulated proteins in the supernatant of ABCB5$^+$ SPs may also be relevant to be explored in future studies. Our choice for ANG was further inspired by our data of impaired signaling from dysfunctional endothelial cells. Akt signaling as well as angiogenic VEGF receptor signaling was suppressed both in the coculture of HUVECs with *db/db* fibroblasts and in vessels harvested from *db/db* mice. In fact, ANG was earlier reported to stimulate *VEGF* mRNA levels (Kishimoto et al., 2005) and, thus as we hypothesized, may counteract suppressed VEGF signaling in diabetes. Lysates from the skin of mice with diabetes depicted severely reduced ANG expression compared with those from the skin of WT mice (Figure 4c and Supplementary Figure S4a). This correlates with suppression of growth signaling, with a severe reduction of activated downstream effectors such as phosphorylated Akt; phosphorylated S6 ribosomal protein, a component of 40S ribosomal subunit involved in translation; and the translation initiation complex protein elf4G (Figure 4c and d and Supplementary Figure S4a and b)—proteins that, independent of ANG, had earlier been shown to be involved in ribosomal biogenesis and protein translation (Holz et al., 2005; Shahbazian et al., 2006; Wang et al., 2001). As expected, our data confirm that ANG when supplied to HUVEC cultures stimulates VEGFR2 signaling, with phosphorylation of the downstream effector c-Src at Tyr416 position. ANG also enforces growth signaling through the phosphorylation of the downstream effector pS6 ribosomal protein (Supplementary Figure S5a and b) involved in enhancing translation and protein biosynthesis required for proliferation, growth, and migration during angiogenesis.

To specifically address the expression of ANG in human diabetic wounds, we performed immunostaining from wound sections (Figure 4e). Interestingly, wound biopsies obtained from patients with chronic diabetic foot ulcers and chronic venous leg ulcers depicted a significant decrease in ANG expression compared with biopsies obtained from acute
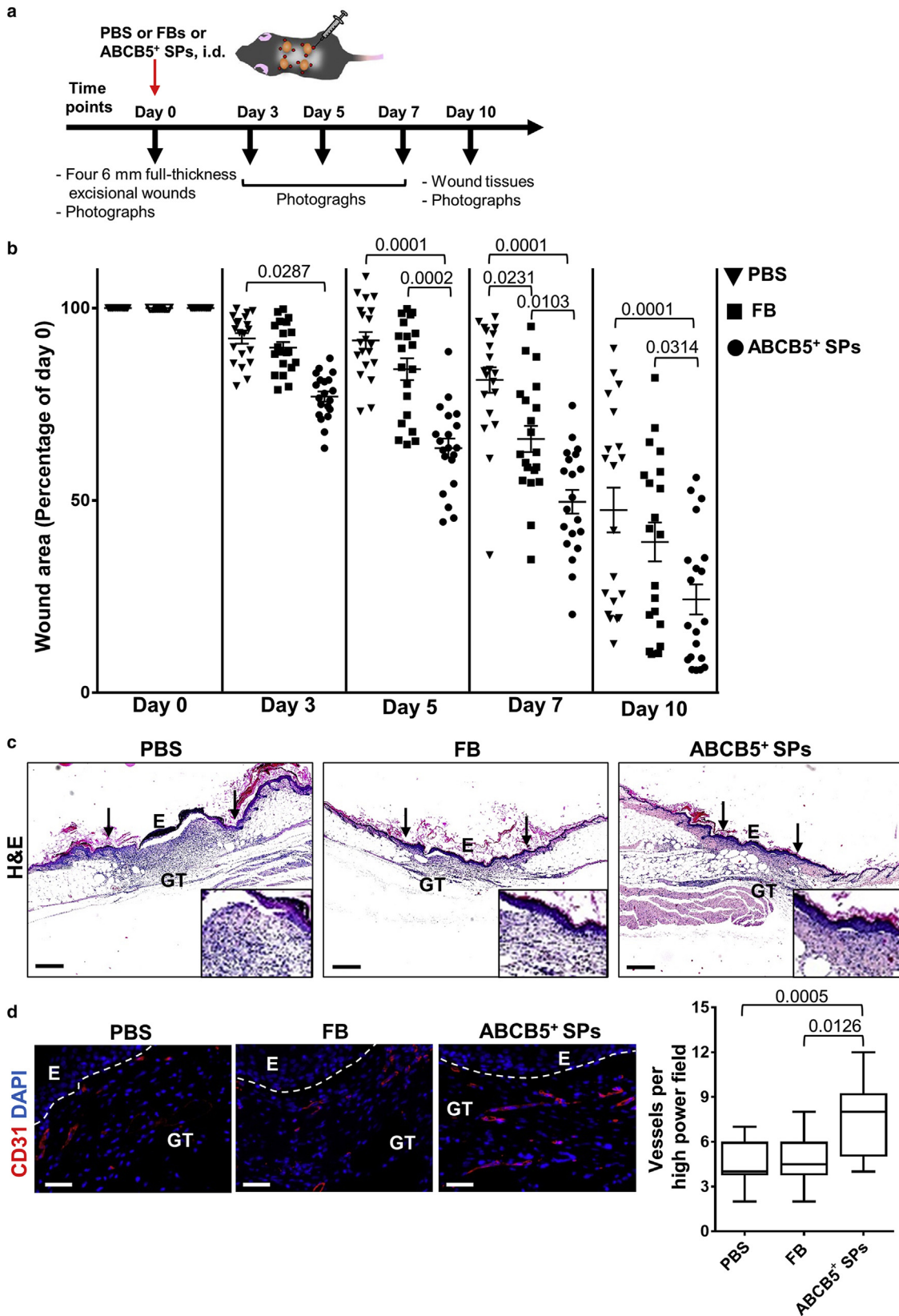
Figure 3. ABCB5^{+} SPs enhance wound healing and stimulate angiogenesis in the wounds of mice with diabetes. (**a**) Scheme showing experimental setting. (**b**) Time kinetics of wound healing in PBS (vehicle)-, FBs-, or ABCB5^{+} SPs–injected wounds of *db/db* mice with diabetes. Statistical analysis was performed using one-way ANOVA; values are represented as mean ± SEM, n = 5. (**c**) Representative H&E photomicrographs depicting wound architecture in PBS (vehicle)-, FBs-, or ABCB5^{+} SPs–injected wounds from mice with diabetes. Bar = 500 μm. (**d**) Immunostaining and quantification of blood vessel formation marked with CD31 (red) in day-10 wounds of *db/db* mice, which had been injected with PBS (vehicle), FBs, or ABCB5^{+} SPs after wounding. Bar = 50 μm (n = 5). Statistical analysis was performed using one-way ANOVA; values are represented as mean ± SEM, n = 5. E, epidermis; FB, fibroblast; GT, granulation tissue; i.d., intradermal; SP, stromal precursor.
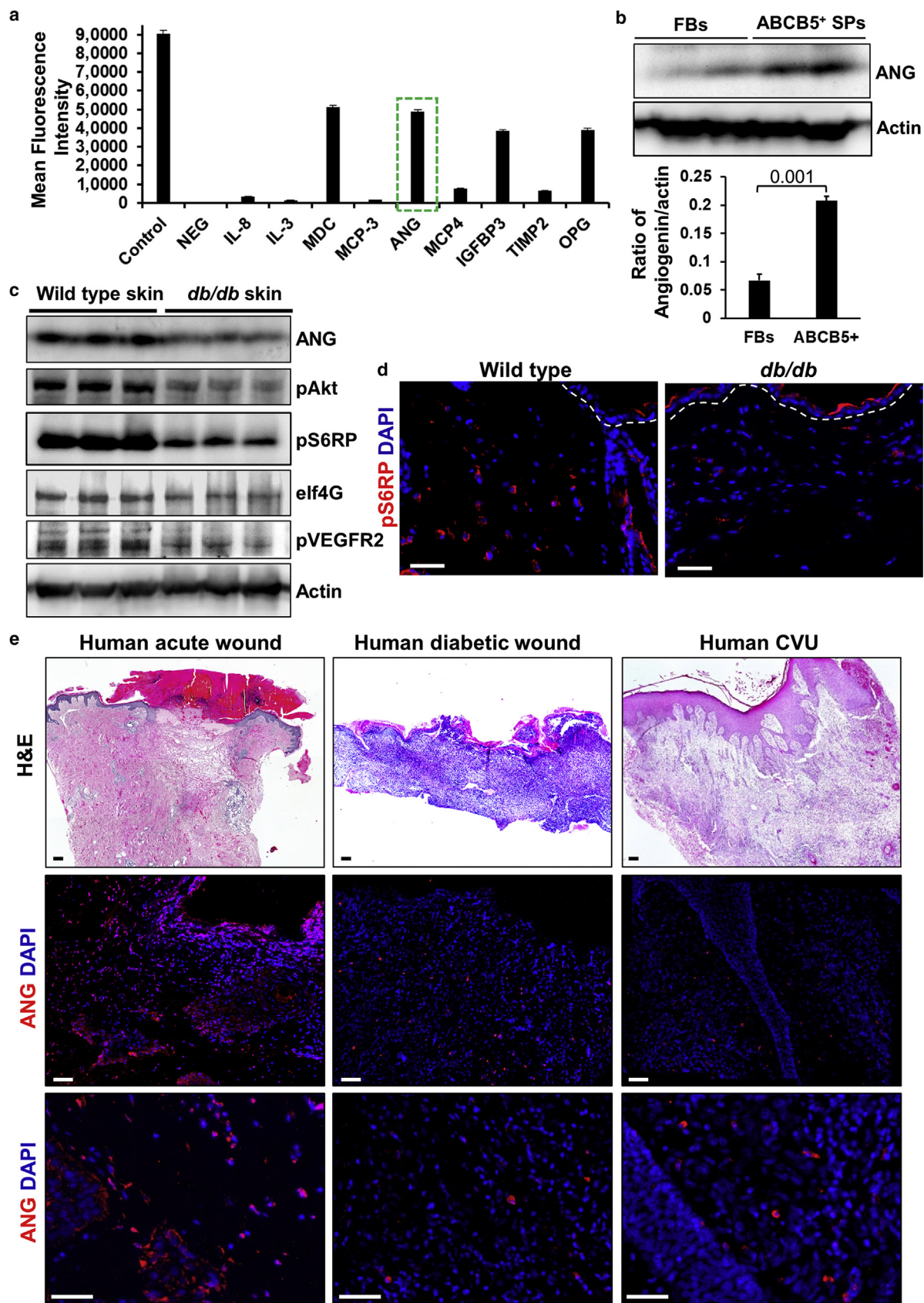
Figure 4. Increased release of ANG from ABCB5$^+$ SPs substitutes low levels of angiogenin and downstream effectors in diabetic skin. (**a**) Secretome analysis of supernatants from ABCB5$^+$ SPs by an antibody array under unstimulated culture conditions. (**b**) Western blot analysis and quantification of ANG in the cell lysates of FBs and ABCB5$^+$ SPs. (**c**) Western blot analysis of ANG and the indicated proteins in skin lysates of wild-type and *db/db* mice. Quantification is shown in Supplementary Figure S4a. (**d**) Immunostaining of pS6RP (red). Its quantification is shown in Supplementary Figure S4b. Bar = 50 µm. (**e**) H&E and

human wounds (Figure 4e and Supplementary Figure S5c and Supplementary Table S1).

Although correlative, these data imply that reduced ANG expression has been conserved across species suffering from chronic wounds.

ANG released by injected ABCB5+ SPs promotes wound healing by enhancing angiogenesis in *db/db* mice

Because ANG plays a prime role in the coordination of angiogenesis and because angiogenesis is a prerequisite for sufficient oxygen and nutrient supply to meet the high energy demand during tissue repair, we next focused on dissecting the role of ANG released from ABCB5+ SPs. The expression of ANG in ABCB5+ is markedly reduced in diabetic skin wounds (Supplementary Figure S6a). The delivery of a high number of ABCB5+ SPs with a fresh reservoir of ANG (Supplementary Figure S6b) in *db/db* wounds not only triggers new blood vessel formation but also significantly accelerates wound closure of otherwise impaired wound closure in mice with diabetes.

To study whether ANG secreted from ABCB5+ SPs is causal for enhanced skin healing of diabetic wounds, we set out to effectively silence ANG through small interfering RNA (siRNA) technologies (Supplementary Figure S6c). PBS, 1×10^6 scrambled siRNA control ABCB5+ SPs, and ANG-silenced ABCB5+ SPs were injected into the edges of full-thickness wounds of *db/db* mice. In addition, we included a group of *db/db* mice that were repetitively injected with 1×10^6 ABCB5+ SPs on days 0, 5, and 10 during wound healing. Analysis of wounds on days 5 and 7 after wounding revealed significantly delayed healing of wounds that had been injected with ANG-silenced ABCB5+ SPs as opposed to that of wounds injected with scrambled siRNA–transfected ABCB5+ SPs (Figure 5a). By contrast, scrambled siRNA–transfected ABCB5+ SPs significantly accelerated wound closure in *db/db* mice on days 5, 7, and 10 compared with that in the PBS-treated *db/db* mice (Figure 5a). These data indicate that ANG is at least in part causal for the therapeutic benefit of ABCB5+ SPs in accelerating impaired wound healing in mice with diabetes, although our data cannot exclude the role of other factors released from ABCB5+ SPs.

Interestingly, repetitive administrations of ABCB5+ SPs also showed improved wound closure in *db/db* mice on days 7 and 10 (Figure 5a) but were less efficient than a single injection of ABCB5+ SPs. It is most likely that multiple injections may interfere with and disrupt the sequentially occurring classical phases of wound healing. In fact, histology of wounds repetitively injected with ABCB5+ SPs depicts a stronger fibrotic response than that of wounds injected with ABCB5+ SPs pretreated with scrambled siRNA or the vehicle control (PBS) (Figure 5b). This suggests that the timing of the application is important to carefully orchestrate appropriate responses.

Immunostaining for the endothelial marker CD31 showed that angiogenesis was severely reduced in sections from wounds injected with ANG-silenced ABCB5+ SPs as opposed to enhanced vessel formation in wounds injected with single or multiple injections of scrambled siRNA-transfected ABCB5+ SPs (Figure 5c and Supplementary Figure S6d).

We also confirmed a causal role of ANG in the in vitro vessel (tube) formation assay where the addition of ABCB5+ SPs to HUVECs and *db/db* murine dermal fibroblasts co-cultures enhanced tube formation as opposed to the co-cultures of HUVECs only with *db/db* murine dermal fibroblasts (Supplementary Figure S6e). By contrast, ABCB5+ SPs silenced for ANG failed to rescue the *db/db* murine dermal fibroblast–dependent impaired tube formation (Supplementary Figure S6e). In addition, collagen deposition indicative of the matrix-restoration phase of wound healing was studied. Interestingly, we found enhanced collagen deposition indicated by blue-colored matrix (Masson's trichrome staining) and enhanced expression of the myofibroblasts marker α-smooth muscle actin in scrambled ABCB5+ SPs-injected wounds compared with that of PBS-injected or ANG-silenced ABCB5+–injected wounds of *db/db* mice (Supplementary Figure S7a and S7b). This partial restoration of key matrix proteins and enhanced expression of α-smooth muscle actin facilitate cellular matrix interaction and support tissue repair and wound contraction of atrophic diabetic dermis. This, in consequence, counteracts wound infection. These results further strengthen our conclusion for a causal role of ANG in ABCB5+ SPs-mediated repair of chronic wounds in *db/db* mice.

In aggregate, our study highlights the therapeutic benefits of ABCB5+ SPs for the successful treatment of nonhealing wounds in a murine model of human type 2 diabetes.

DISCUSSION
The major finding of our study is that the injection of ABCB5+ SPs in a therapeutic intent markedly enhanced angiogenesis and accelerated the overall healing of chronic diabetic wounds. We identified the ribonuclease family member ANG secreted from ABCB5+ SPs at the wound site as a key mediator enforcing new vessel formation in a paracrine manner, thereby restoring impaired wound healing in mice with diabetes (graphical summary). This finding is of outstanding clinical relevance given that angiogenesis is severely suppressed in patients suffering from diabetic nonhealing wounds.

Our data show that the stromal microenvironment of endothelial cells is essential for angiogenesis and, if compromised such as in diabetes mellitus, leads to suppression of tube formation as the most important prerequisite for angiogenesis. In support of this view, our results show that in skin wounds of *db/db* mice, vessel formation is severely reduced in an overall structurally changed skin. The suppressive impact of *db/db* mice fibroblasts on vessel formation was highlighted in an in vitro angiogenesis assay. Although the angiogenesis-suppressing factors from *db/db* stroma have not been explored in this study, we found that the endothelial signature in response to their noxious

---

immunostaining of ANG (red) in human acute, diabetic, and CVU wound biopsies. Bar = 100 μm. Quantification of ANG-positive cells is shown in Supplementary Figure S5c. ANG, angiogenin; CVU, chronic venous leg ulcer; FB, fibroblast; pAkt, phosphorylated protein kinase B; pS6RP, phosphorylated S6RP; pVEGFR2, phosphorylated VEGF receptor 2; SP, stromal precursor.
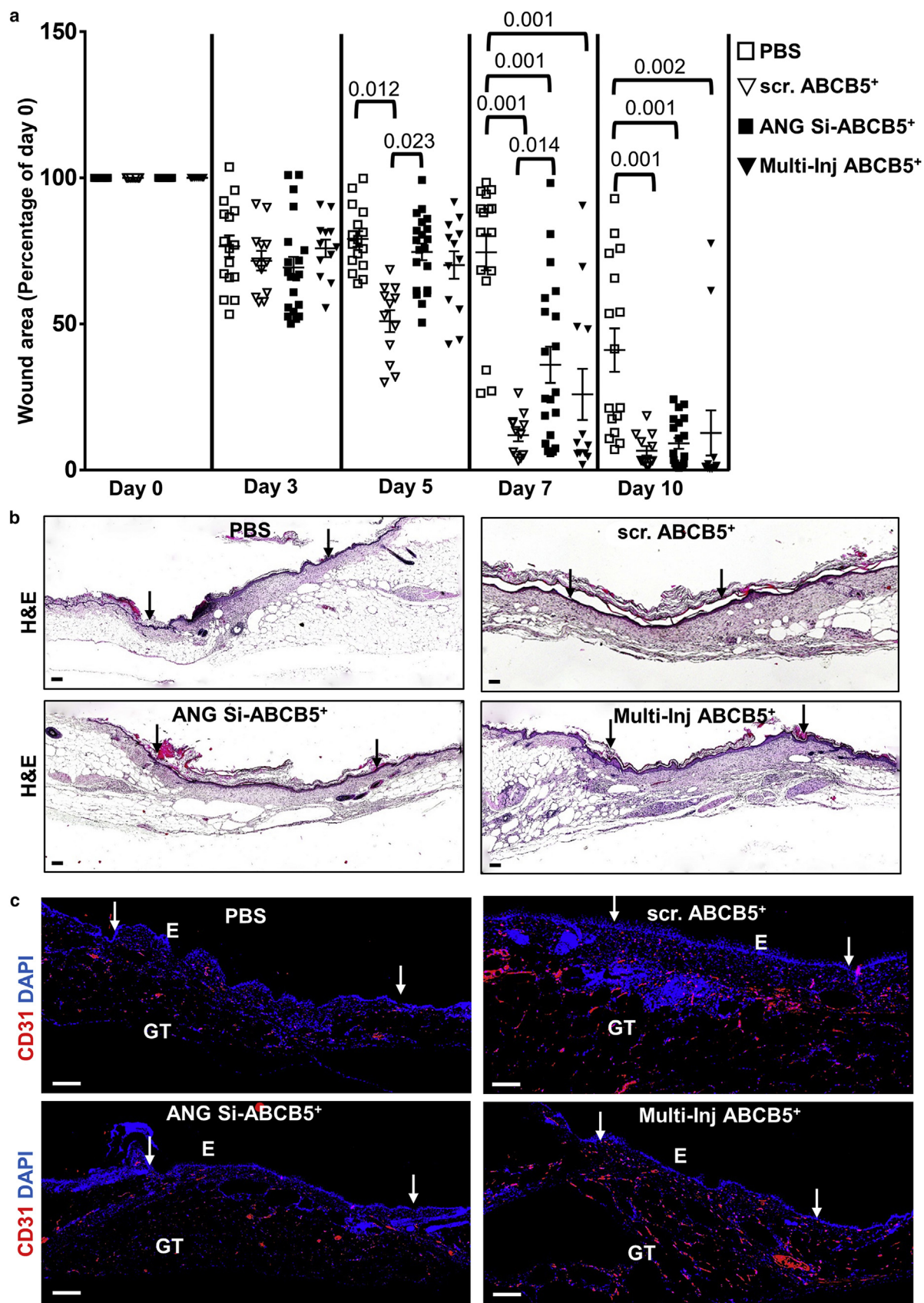
Figure 5. Silencing of ANG abrogates therapeutic beneficial effects of ABCB5⁺ SPs on wound closure in mice with diabetes. (a) Comparison of wound closure after a single injection of PBS (vehicle control) or scrambled ABCB5⁺ SPs or ANG-silenced (ANGSi) ABCB5⁺ SPs or multiple injections of ABCB5⁺ SPs (Multi-inj ABCB5⁺) into wounds of *db/db* mice with diabetes. Statistical analysis was performed using one-way ANOVA; values are represented as mean ± SEM, n = 5. (b) Representative H&E photomicrographs depicting wound architecture in the indicated groups. Bar = 100 μm. (c) Immunostaining of the blood vessel–specific

impact shares the suppression of VEGF and Akt signaling with the endothelial cell signature of vessels from mice with diabetes, and this is also true for upregulated pathways, including apoptosis, DNA damage, and matrix degradation, among others. The number of ABCB5^{+}SPs as well as other SP populations, including PDGFRβ^{+}, Nestin^{+}, and CD34^{+}, are reduced in the skin of mice with diabetes, adding to profound changes in the stromal niche of the skin of mice with diabetes. Therefore, local transplantation of precursor cells holds substantial promise to rebalance the endogenous stromal niche and resident cells therein and may even be appropriate to refine the treatment of nonhealing wounds (Goncalves et al., 2016; Silberstein et al., 2016).

Our study uncovered ANG released from injected stromal ABCB5^{+} SPs at the wound site to be causal for the impressive rescue of both impaired angiogenesis and the nonhealing state of wounds in mice with diabetes. Alternatively, approaches such as delivery of ANG by either recombinant protein or an expression vector need to be further assessed in preclinical and clinical settings. Earlier, reduced ANG concentrations were found in the serum of patients suffering from diabetes mellitus (Siebert et al., 2010). In this study, we show that ANG is also markedly less expressed in human diabetic wounds and in chronic venous leg ulcers. Thus, reduced ANG levels are conserved across species suffering from chronic wounds, although the role of ANG in human wounds needs to be further explored. Accordingly, ANG was identified to promote cancer, and this knowledge has propelled the development of anticancer therapies (Shapiro et al., 1987). Variants and sequence variations of ANG have been linked to Parkinson's disease (Steidinger et al., 2011), Alzheimer's disease (Kim and Kim, 2012), and diabetic peripheral neuropathy (Greenway et al., 2006; van Es et al., 2009; Wang et al., 2013).

Classically, after entry into endothelial cells through receptor-mediated endocytosis (Ferguson and Subramanian, 2018), ANG translocates into the nucleus and subsequently into the nucleolus where it stimulates ribosomal RNA transcription, most important for ribosomal biogenesis and the control of transcription of other angiogenic factors and GFs (Ibaragi et al., 2009; Kishimoto et al., 2005). Interestingly, we provide data that ANG not only activates VEGF receptor signaling but also stimulates Akt downstream signaling in HUVECs. ANG released from ABCB5^{+} SPs is vital for angiogenesis in a diabetic microenvironment installed by insulin-resistant *db/db* mice stroma (Shao et al., 2000). This restored endothelial cell function may either be due to the unlocking of VEGF signaling or due to a receptor-independent direct cytoplasmic signaling. A limitation of the employed xenograft model is that it does not allow for the study of engraftment and differentiation of injected ABCB5^{+} SPs.

Our data on the successful therapy with ABCB5^{+}-derived SPs for the treatment of nonhealing diabetic wounds have substantial clinical relevance for intended implementation into clinical routine. The employment of a single marker strategy (ABCB5^{+}) allows the enrichment of an easily accessible homogeneous ABCB5^{+}-derived SP population from human skin with Good Manufacturing Practice grade quality, reliable potency ready to use for clinical routine (Tappenbeck et al., 2019; Vander Beken et al., 2019). Thus, the dermal ABCB5^{+} SPs described in this study hold substantial promise for the successful clinical therapy of non-healing diabetic wounds. In fact, clinical phase IIA studies have recently been initiated (EudraCT number: 2015-000399-81, 2017-000233-31, 000234-57), with promising results of the first studied patients suffering from diabetic foot ulcers.

MATERIALS AND METHODS
For detailed methods, see the Supplementary Materials and Methods.

Mice experiments
For wound healing studies, male *db/db* mice with diabetes (*BKS.Cg-Dock7m+/+ Leprdb/J*) and WT mice (C57BLKS/J) aged 8–10 weeks were used. Mice were directly purchased from Jackson Laboratory (Bar Harbor, ME) and housed under pathogen-free conditions at the animal care facility of Ulm University (Ulm, Germany) in compliance with the German Law for Welfare of Laboratory Animals. All experiments were approved by the RP Tübingen Baden-Württemberg (approval number TVA1289).

Histology and immunostaining
Histology and immunostainings were performed on 5-μm thick wound sections or sections from nonwounded skin biopsies by standard procedures, as previously described (Singh et al., 2017). We employed primary antibodies against ABCB5 (TICEBA GmbH, Heidelberg, Germany and Thermo Fisher Scientific, Waltham, MA), CD34 (eBioscience, Waltham, MA), CD31, PS6RP, PDGFRβ (Cell Signaling Technology, Danvers, MA), and ANG and α-smooth muscle actin (R&D Systems, Minneapolis, MN). Respective isotypes were used as negative controls, and AF488- and AF555-conjugated (Life Technologies, Carlsbad, CA) or horseradish peroxidase—conjugated secondary antibodies (Vector Laboratories, Inc., Burlingame, CA) were employed. Nuclei were counterstained with DAPI. After staining, tissues were mounted with fluorescence mounting medium (Dako GmbH, Jena, Germany). Images were captured by Zeiss Axiophot microscope equipped with an AxioCam digital color camera, Zen 3.2 (ZEN lite) and AxioVision software, version 4.8 (Carl Zeiss, Oberkochen, Germany).

Statistical calculations
Error bars represent SEM. The significance of differences between two groups was analyzed by Student's *t*-test or one-way ANOVA, followed by Bonferroni correction for comparing the difference between more than two groups and is presented as absolute *P*-values.

Data availability statement
RNA-sequencing analyses data has been deposited in the Gene Expression Omnibus with accession number GSE181881. Additional data related to this paper may be requested from the corresponding author.

---

marker CD31 (red) in wounds from the indicated groups. Quantification of CD31 is depicted in Supplementary Figure S6d. Nuclei were stained with DAPI (blue). Bar = 200 μm. (n = 5). Wound edges are marked with arrows. ANG, angiogenin; E, epidermis; GT, granulation tissue; scr, scrambled; inj, injections; Multi, multiple; Si, silenced; SP, stromal precursor.

ORCIDs
Karmveer Singh: http://orcid.org/0000-0002-1237-7417
Pallab Maity: http://orcid.org/0000-0001-9769-3533
Albert Kallon Koroma: http://orcid.org/0000-0001-5579-0845
Abhijit Basu: http://orcid.org/0000-0002-7176-250X
Rajeev Kumar Pandey: http://orcid.org/0000-0002-1368-323X
Seppe Vander Beken: http://orcid.org/0000-0002-1457-6591
Philipp Haas: http://orcid.org/0000-0003-4802-0601
Linda Krug: http://orcid.org/0000-0001-5486-9770
Adelheid Hainzl: http://orcid.org/0000-0003-1131-3144
Anca Sindrilaru: http://orcid.org/0000-0002-1691-0047
Christiane Pfeiffer: http://orcid.org/0000-0001-7770-168X
Meinhard Wlaschek: http://orcid.org/0000-0001-5821-1140
Natasha Y. Frank: http://orcid.org/0000-0001-8196-0449
Markus H. Frank: http://orcid.org/0000-0002-1312-0488
Christoph Ganss: http://orcid.org/0000-0003-0396-6591
András Bánvölgyi: http://orcid.org/0000-0002-7071-1364
Norbert Wikonkál: http://orcid.org/0000-0003-4949-8711
Sabine Eming: http://orcid.org/0000-0001-8485-3921
Irena Pastar: http://orcid.org/0000-0003-0197-6198
Marjana Tomic-Canic: http://orcid.org/0000-0002-9341-0193
Mark A. Kluth: http://orcid.org/0000-0003-0764-4645
Karin Scharffetter-Kochanek: http://orcid.org/0000-0002-9655-685X

SUPPLEMENTARY MATERIAL
Supplementary material is linked to the online version of the paper at www.jidonline.org, and at https://doi.org/10.1016/j.jid.2021.10.026.

REFERENCES
Aldworth J, Patterson C, Jacobs E, Misra A, Tamayo T, Snouffer E, et al. IDF diabetes atlas. 8th, edition. Brussels, Belgium: International Diabetes Federation; 2017.

Armstrong DG, Swerdlow MA, Armstrong AA, Conte MS, Padula WV, Bus SA. Five year mortality and direct costs of care for people with diabetic foot complications are comparable to cancer. J Foot Ankle Res 2020;13:16.

Augustin M, Vanscheidt W. Chronic venous leg ulcers: the future of cell-based therapies. Lancet 2012;380:953—5.

Chen H, Charlat O, Tartaglia LA, Woolf EA, Weng X, Ellis SJ, et al. Evidence that the diabetes gene encodes the leptin receptor: identification of a mutation in the leptin receptor gene in db/db mice. Cell 1996;84:491—5.

Cho S, Beintema JJ, Zhang J. The ribonuclease A superfamily of mammals and birds: identifying new members and tracing evolutionary histories. Genomics 2005;85:208—20.

Davey GC, Patil SB, O'Loughlin A, O'Brien T. Mesenchymal stem cell-based treatment for microvascular and secondary complications of diabetes mellitus. Front Endocrinol 2014;5:86.

Ferguson R, Subramanian V. The cellular uptake of angiogenin, an angiogenic and neurotrophic factor is through multiple pathways and largely dynamin independent. PLoS One 2018;13:e0193302.

Goncalves KA, Silberstein L, Li S, Severe N, Hu MG, Yang H, et al. Angiogenin promotes hematopoietic regeneration by dichotomously regulating quiescence of stem and progenitor cells. Cell 2016;166:894—906.

Greenway MJ, Andersen PM, Russ C, Ennis S, Cashman S, Donaghy C, et al. ANG mutations segregate with familial and 'sporadic' amyotrophic lateral sclerosis. Nat Genet 2006;38:411—3.

Holz MK, Ballif BA, Gygi SP, Blenis J. mTOR and S6K1 mediate assembly of the translation preinitiation complex through dynamic protein interchange and ordered phosphorylation events. Cell 2005;123:569—80.

Ibaragi S, Yoshioka N, Kishikawa H, Hu JK, Sadow PM, Li M, et al. Angiogenin-stimulated rRNA transcription is essential for initiation and survival of AKT-induced prostate intraepithelial neoplasia. Mol Cancer Res 2009;7:415—24.

Jiang D, Qi Y, Walker NG, Sindrilaru A, Hainzl A, Wlaschek M, et al. The effect of adipose tissue derived MSCs delivered by a chemically defined carrier on full-thickness cutaneous wound healing. Biomaterials 2013;34:2501—15.

Kim YN, Kim DH. Decreased serum angiogenin level in Alzheimer's disease. Prog Neuropsychopharmacol Biol Psychiatry 2012;38:116—20.

Kishimoto K, Liu S, Tsuji T, Olson KA, Hu GF. Endogenous angiogenin in endothelial cells is a general requirement for cell proliferation and angiogenesis. Oncogene 2005;24:445—56.

Koliaraki V, Prados A, Armaka M, Kollias G. The mesenchymal context in inflammation, immunity and cancer. Nat Immunol 2020;21:974—82.

Meyer P, Maity P, Burkovski A, Schwab J, Müssel C, Singh K, et al. A model of the onset of the senescence associated secretory phenotype after DNA damage induced senescence. PLoS Comput Biol 2017;13:e1005741.

Okonkwo UA, Chen L, Ma D, Haywood VA, Barakat M, Urao N, et al. Compromised angiogenesis and vascular Integrity in impaired diabetic wound healing. PLoS One 2020;15:e0231962.

Qi Y, Jiang D, Sindrilaru A, Stegemann A, Schatz S, Treiber N, et al. TSG-6 released from intradermally injected mesenchymal stem cells accelerates wound healing and reduces tissue fibrosis in murine full-thickness skin wounds. J Invest Dermatol 2014;134:526—37.

Ressler S, Bartkova J, Niederegger H, Bartek J, Scharffetter-Kochanek K, Jansen-Dürr P, et al. p16INK4A is a robust in vivo biomarker of cellular aging in human skin. Aging Cell 2006;5:379—89.

Riordan JF. Angiogenin. Methods Enzymol 2001;341:263—73.

Schatton T, Yang J, Kleffel S, Uehara M, Barthel SR, Schlapbach C, et al. ABCB5 identifies immunoregulatory dermal cells. Cell Rep 2015;12:1564—74.

Shahbazian D, Roux PP, Mieulet V, Cohen MS, Raught B, Taunton J, et al. The mTOR/PI3K and MAPK pathways converge on eIF4B to control its phosphorylation and activity. EMBO J 2006;25:2781—91.

Shao J, Yamashita H, Qiao L, Friedman JE. Decreased Akt kinase activity and insulin resistance in C57BL/KsJ-Leprdb/db mice. J Endocrinol 2000;167:107—15.

Shapiro R, Strydom DJ, Olson KA, Vallee BL. Isolation of angiogenin from normal human plasma. Biochemistry 1987;26:5141—6.

Siebert J, Reiwer-Gostomska M, Mysliwska J, Marek N, Raczynska K, Glasner L. Glycemic control influences serum angiogenin concentrations in patients with type 2 diabetes. Diabetes Care 2010;33:1829—30.

Silberstein L, Goncalves KA, Kharchenko PV, Turcotte R, Kfoury Y, Mercier F, et al. Proximity-based differential single-cell analysis of the niche to identify stem/progenitor cell regulators. Cell Stem Cell 2016;19:530—43.

Singh K, Krug L, Basu A, Meyer P, Treiber N, Vander Beken S, et al. Alpha-ketoglutarate curbs differentiation and induces cell death in mesenchymal stromal precursors with mitochondrial dysfunction. Stem Cells 2017;35:1704—18.

Soria-Juan B, Escacena N, Capilla-González V, Aguilera Y, Llanos L, Tejedo JR, et al. Cost-effective, safe, and personalized cell therapy for critical limb ischemia in type 2 diabetes mellitus [published correction appears in Front Immunol 2020;11:2029]. Front Immunol 2019;10:1151.

Steidinger TU, Standaert DG, Yacoubian TA. A neuroprotective role for angiogenin in models of Parkinson's disease. J Neurochem 2011;116:334–41.

Tahergorabi Z, Khazaei M. Imbalance of angiogenesis in diabetic complications: the mechanisms. Int J Prev Med 2012;3:827–38.

Tappenbeck N, Schröder HM, Niebergall-Roth E, Hassinger F, Dehio U, Dieter K, et al. In vivo safety profile and biodistribution of GMP-manufactured human skin-derived ABCB5-positive mesenchymal stromal cells for use in clinical trials. Cytotherapy 2019;21:546–60.

Thavorn K, van Katwyk S, Krahn M, Mei SHJ, Stewart DJ, Fergusson D, et al. Value of mesenchymal stem cell therapy for patients with septic shock: an early health economic evaluation. Int J Technol Assess Health Care 2020;36:525–32.

van Es MA, Diekstra FP, Veldink JH, Baas F, Bourque PR, Schelhaas HJ, et al. A case of ALS-FTD in a large FALS pedigree with a K17I ANG mutation [published correction appears in Neurology 2009;72:774]. Neurology 2009;72:287–8.

Vander Beken S, de Vries JC, Meier-Schiesser B, Meyer P, Jiang D, Sindrilaru A, et al. Newly defined ATP-binding cassette subfamily B member 5 positive dermal mesenchymal stem cells promote healing of chronic iron-overload wounds via secretion of interleukin-1 receptor antagonist. Stem Cells 2019;37:1057–74.

Wang H, Fan D, Zhang Y. Angiogenin gene polymorphism: a risk factor for diabetic peripheral neuropathy in the northern Chinese Han population. Neural Regen Res 2013;8:3434–40.

Wang X, Li W, Williams M, Terada N, Alessi DR, Proud CG. Regulation of elongation factor 2 kinase by p90(RSK1) and p70 S6 kinase. EMBO J 2001;20:4370–9.

Xiao Y, Reis LA, Feric N, Knee EJ, Gu J, Cao S, et al. Diabetic wound regeneration using peptide-modified hydrogels to target re-epithelialization. Proc Natl Acad Sci USA 2016;113:E5792–801.

SUPPLEMENTARY MATERIALS AND METHODS

Wound healing model

Mice were anesthetized using ketamine (100 mg/ml) and xylazine (10 mg/ml) by intraperitoneal injections (10 µl/g body weight) or by inhalational anesthesia sevoflurane. The dorsal skin of mice was shaved and cleaned, followed by inflicting four full-thickness excisional wounds using 6-mm round biopsy punches (STIEFEL, Offenbach, Germany). Thereafter, vehicle, 1×10^6 of either human dermal fibroblasts, young human skin–derived ABCB5$^+$, or small interfering RNA–treated stromal precursors were injected into wound margins. The therapeutic ABCB5$^+$ derived from healthy young human individuals and isolated with a single marker strategy (ABCB5$^+$) and enriched to an easily accessible homogeneous ABCB5$^+$ stromal precursor population with Good Manufacturing Practice grade quality.

Wound closure was documented by capturing the photographs of each wound on 0, 3, 5, 7, and 10 days. Wound areas of each mouse were then calculated using Photoshop software (version 7.0) (Adobe Systems, San Jose, CA). For histology and molecular biology analysis, wound tissues were harvested and fixed in 4% paraformaldehyde or stored at −80 °C.

Human wound tissue collection

Full-thickness diabetic foot ulcer tissue was obtained from consenting patients (n = 4, mean age ± SD = 60.5 ± 5.97) receiving standard care at the University of Miami Hospital Wound Clinic (FL), as previously described (Ramirez et al., 2018; Sawaya et al., 2020). The protocols, including written informed consent, were approved by the university Institutional Review Board (protocols #20140473 and #20090709). Ulcers did not have any clinical signs of infection. Full-thickness diabetic ulcers were also obtained from the University of Cologne (Cologne, Germany), and all investigations were performed after approval of the institution's human research review committee of the University of Cologne (registration number 08-144). Informed written consent was obtained from each subject. Chronic venous leg ulcers were collected at the Department of Dermatology, Dermatooncology and Venerology, Semmelweis University (Budapest, Hungary) (registration number 10080/2015). The acute wounds were obtained from healthy young volunteers; the protocols were approved by the University Hospital Institutional Review Board (Ulm, Germany) (registration number 225/2002). The tissue was fixed in formalin immediately after collection for subsequent paraffin embedding.

In vitro angiogenesis assays

The in vitro angiogenesis assay was performed by coculturing human vascular endothelial cells on top of human or mouse dermal fibroblast monolayers in six-well plates at 5% carbon dioxide, 21% oxygen, and 37 °C. We maintained this coculture for 14 days to stimulate angiogenesis. At the end of 14 days, newly formed vessels were fixed with 4% perfluoroalkoxy alkane, and rate of angiogenesis was quantified after immunostaining for the endothelial-specific marker CD31 in all studied experimental groups.

Antibody array

An antibody array coated with 80 different antibodies (Ray-Bio Human Cytokine Antibody Array G-Series 5; RayBiotech, Peachtree Corners, GA) was used to detect numerous proteins released from ABCB5$^+$ stromal precursors into the culture supernatant during a period of 72 hours. Then, the signal intensity of individual spots was calculated using image analysis software.

Western blotting

Western blot analyses were performed as previously described (Singh et al., 2015). Briefly, after protein transfer, the nitrocellulose membranes were incubated with primary antibodies against angiogenin (R&D system, Minneapolis, MN), actin, p16 (Santa Cruz Biotechnology, Dallas, TX), phosphorylated protein kinase B, p21, phosphorylated S6RP, elf4G, phosphorylated VEGFR2, pSrc, cleaved caspase-3 (Cell Signaling Technology, Danvers, MA), collagen I, and collagen III (Novus Biologicals, Littleton, CO). This was followed by incubation with horseradish peroxidase—conjugated secondary antibodies that were purchased from (Jackson ImmunoResearch, West Grove, PA). The membranes were developed by LumiGLO substrate (Cell Signaling Technology, Danvers, MA) using Vilber Fusion chemiluminescence imaging system.

Whole transcriptomic analysis by RNA-sequencing

RNA was isolated using RNeasy micro kit (Qiagen, Hilden, Germany) from FACS-sorted human vascular endothelial cells that were cocultured with either wild-type or *db/db* murine dermal fibroblasts for 5 days as well as from veins and arteries of wild-type and *db/db* mice. Before RNA-sequencing analysis, RNA quality control was done by Bioanalyzer or Qiaxcel, and RNA samples showing RNA integrity numbers between 8 and 10 were considered for further steps (Singh et al., 2018).

RNA-sequencing library preparation and sequencing

High-quality RNA from different experimental groups was subjected for ribosomal RNA depletion using RiboMinus Eukaryote System version 2 kit (Thermo Fisher Scientific, Waltham, MA). The ribosomal RNA—depleted RNA was then used for library preparation. Libraries were prepared by NEBNext Ultra II Directional RNA Library Prep Kit (New England Biolabs, Ipswich, MA). RNA-sequencing libraries were checked for quality using Tape station (Agilent Technologies, Santa Clara, CA), and libraries were quantified using Qubit (Thermo Fisher Scientific). Equimolar pooled libraries were sequenced in Novaseq using S1/S2 flow cells (2 × 100 pair-end reads). For data processing, demultiplexed fastq reads were aligned using Hisat2, and transcripts were assembled using cufflinks, and differential expression analyses were performed using cuffdiff. Data were visualized and presented in rstudio environment using cummerbund package and customized scripts.

Pathway enrichment analysis and hierarchical clustering

To extract the information from sequencing reads, bioinformatic analysis was performed as described earlier (Singh et al., 2018).

SUPPLEMENTARY REFERENCES

Ramirez HA, Pastar I, Jozic I, Stojadinovic O, Stone RC, Ojeh N, et al. Staphylococcus aureus triggers induction of miR-15B-5P to diminish DNA repair and deregulate inflammatory response in diabetic foot ulcers. J Invest Dermatol 2018;138:1187—96.

Sawaya AP, Stone RC, Brooks SR, Pastar I, Jozic I, Hasneen K, et al. Deregulated immune cell recruitment orchestrated by FOXM1 impairs human diabetic wound healing. Nat Commun 2020;11:4678.

Singh K, Camera E, Krug L, Basu A, Pandey RK, Munir S, et al. JunB defines functional and structural integrity of the epidermo-pilosebaceous unit in the skin. Nat Commun 2018;9:3425.

Singh K, Maity P, Krug L, Meyer P, Treiber N, Lucas T, et al. Superoxide anion radicals induce IGF-1 resistance through concomitant activation of PTP1B and PTEN. EMBO Mol Med 2015;7:59—77.
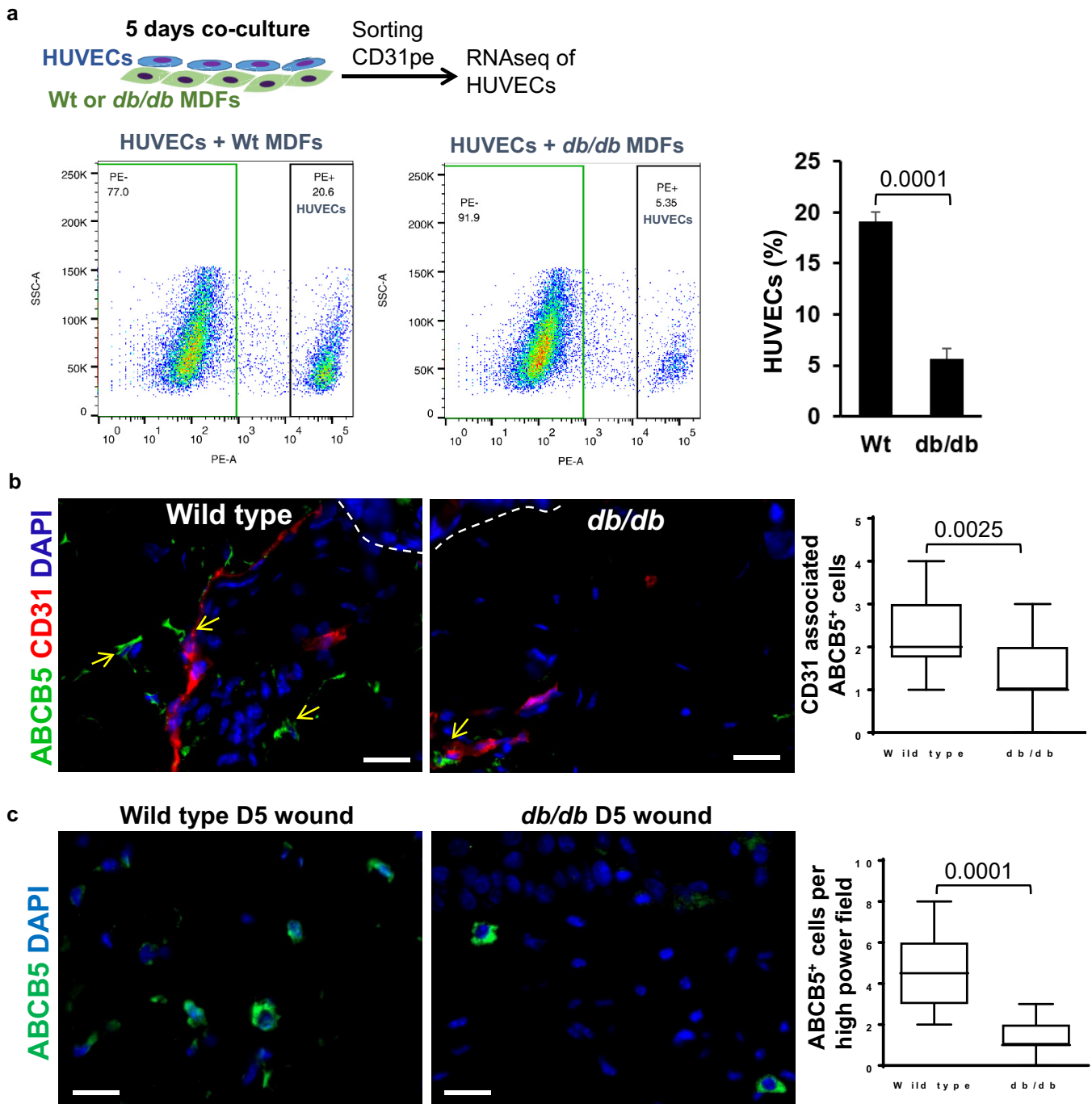
Supplementary Figure S1. *db/db* **mouse fibroblasts attenuate HUVECs survival.** (**a**) FACS analysis depicting a reduction of HUVECs ratio after 5 Ds of coculture with *db/db* mouse fibroblasts as opposed to HUVECs cocultured with WT mouse fibroblasts. An equal number of HUVECs (1×10^6) were seeded at the beginning of coculture. Statistical analysis was performed using unpaired *t*-test; values are represented as mean ± SEM, n = 3. (**b**) Immunostaining and quantification of ABCB5^{+} precursors (green) and CD31 (red) in the skin of WT mice and that of mice with diabetes. Nuclei were stained with DAPI (blue). Bar = 20 μm. (**c**) Immunostaining and quantification of ABCB5^{+} precursors (green) in the wounds of WT mice and mice with diabetes. Nuclei were stained with DAPI (blue). Bar = 20 μm. D, day; HUVEC, human umbilical vein endothelial cell; MDF, murine dermal fibroblast; PE-A, phycoerythrin-area; RNAseq, RNA-sequencing; SSC-A, side scatter area; WT, wild type.
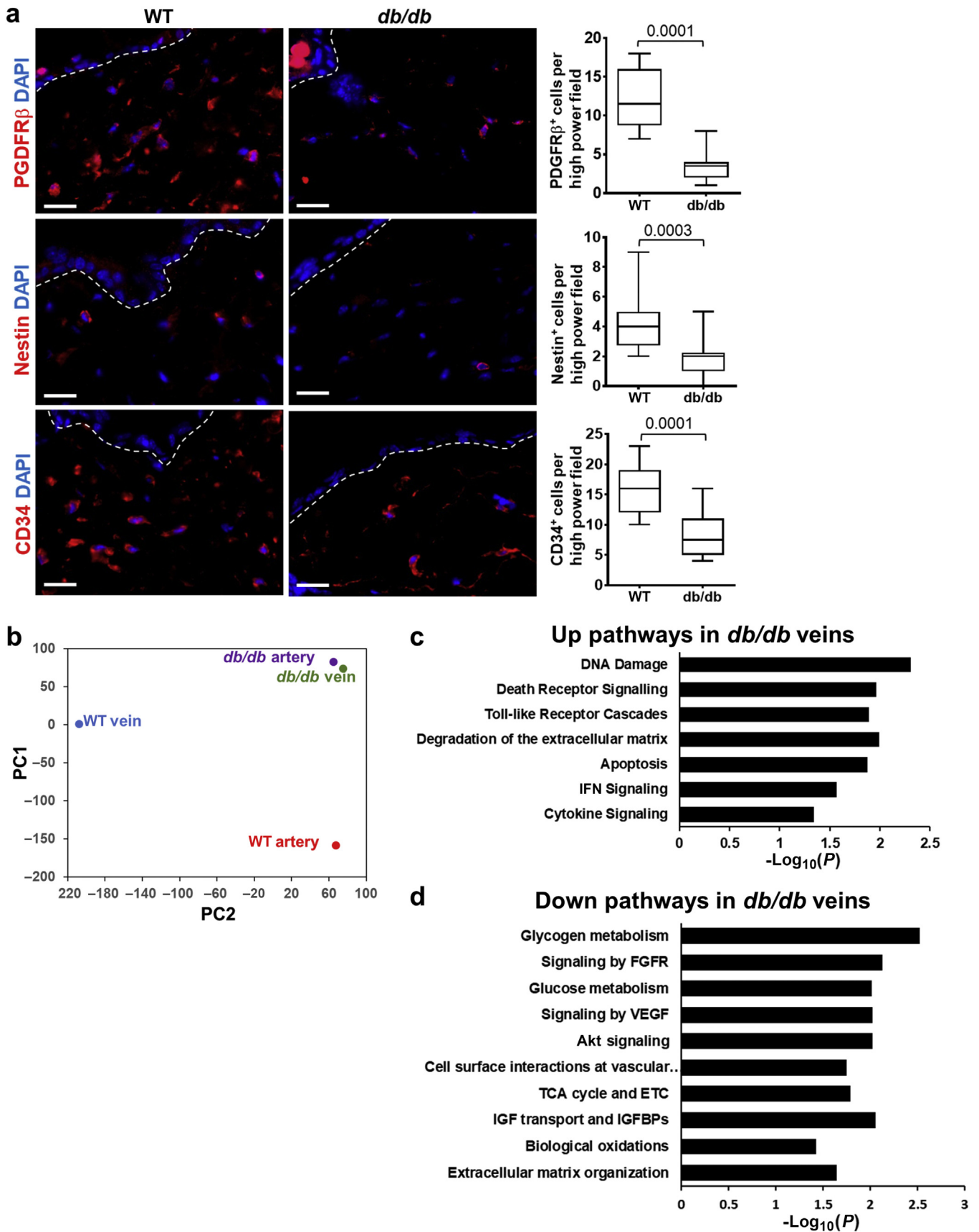
Supplementary Figure S2. Dermal precursors decline and vascular network undergoes remodeling during diabetes. (**a**) Immunostaining and quantification of PDGFRβ, Nestin, and CD34 (red) marking dermal precursor subsets in WT and *db/db* mouse dermis. Nuclei were stained with DAPI (blue). Bar = 20 μm. Statistical analysis was performed using unpaired *t*-test; values are represented as mean ± SEM, n = 3. (**b**) PCA plot depicting the clusters of WT and *db/db* mice

a
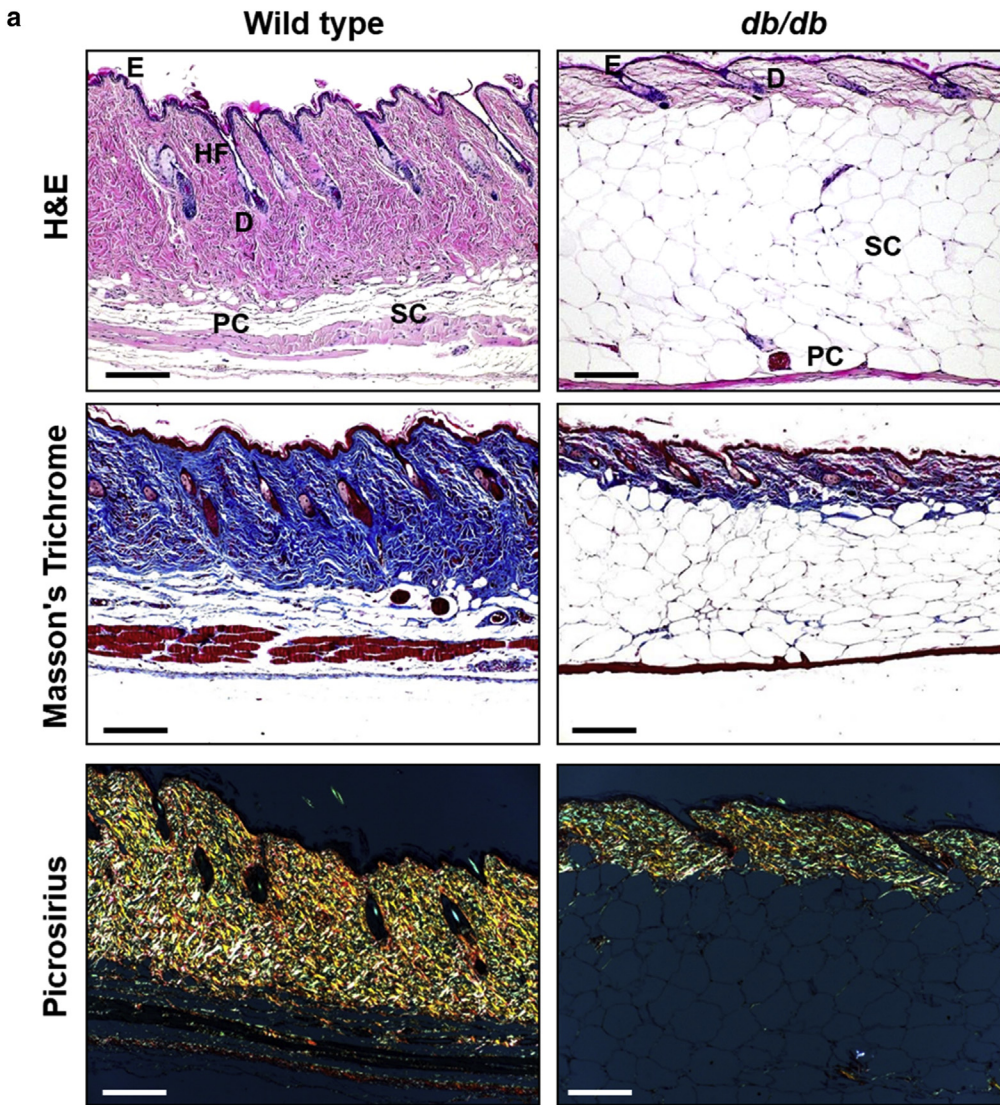
Supplementary Figure S3. Obesity-induced diabetes severely affects skin homeostasis and architecture. (**a**) Representative H&E-stained microphotographs depicting the histology of dorsal skin from WT and *db/db* mouse (upper panel). Collagen fibers stained blue in Masson's trichrome staining (middle panel). The images by polarized microscope obtained after picrosirus staining display thin fibers in green and thick fibers in yellow color (lower panel). Collagen is severely reduced with a remarkable decrease in thick collagen fibers in *db/db* mice. Bar = 200 μm. (**b**) Densitometry analysis of western blots shown in Figure 2f. The ratio of the studied protein with actin was assessed. Statistical analysis was performed using unpaired *t*-test; values are represented as mean ± SEM, n = 3. Col collagen; D, dermis; E, epidermis; HF, hair follicle; pAkt, phosphorylated protein kinase B; PC, panniculus carnosus; SC, subcutaneous layer; WT, wild type.

b
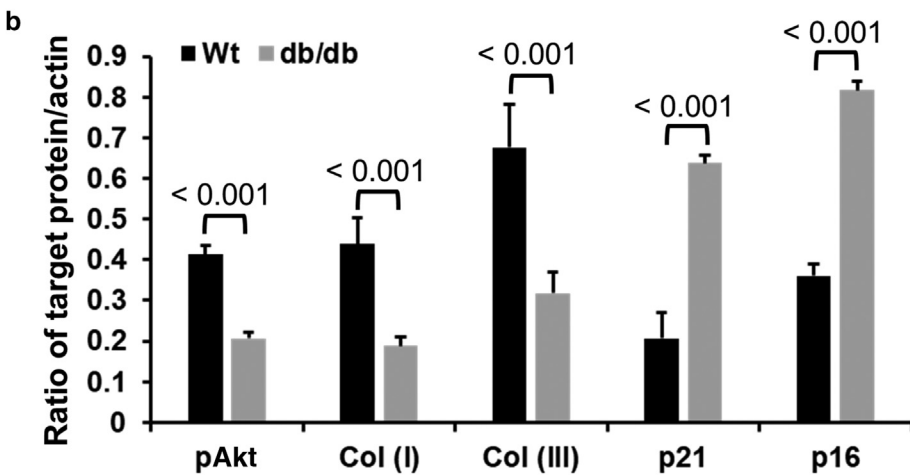
arteries or veins on the basis of their similarity in gene expression. (**c**) Pathway enrichment analysis showing the key significantly enriched signaling pathways, which are upregulated or (**d**) downregulated in *db/db* mice veins compared with that in WT veins. Akt, protein kinase B; ETC, electron transport chain; PC, principal component; PCA, principal component analysis; TCA, tricarboxylic acid; WT, wild type.
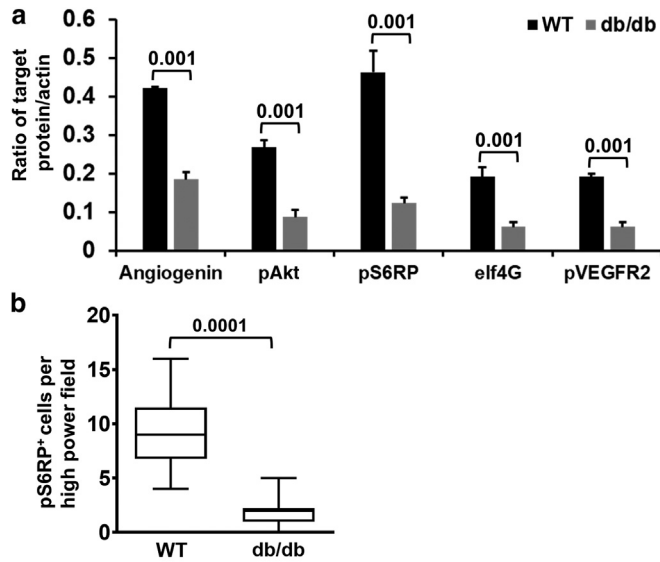
Supplementary Figure S4. Angiogenin expression declines in chronic human wounds. (**a**) Densitometric analysis of western blots in Figure 4c depicting angiogenin and effectors of insulin (pAkt, pRPS6, elf4G, and pVEGFR2) signaling in WT and *db/db* mouse skin lysates. (**b**) Quantification of pS6RP-positive cells shown in Figure 4d in the dermal compartment from WT and *db/db* mouse skin. Statistical analysis was performed using unpaired *t*-test; values are represented as mean ± SEM, n = 3. pAkt, phosphorylated protein kinase B; pRPS6, phosphorylated RPS6; pVEGFR2, phosphorylated VEGF receptor 2; WT, wild type.

a

b

c

Supplementary Figure S5. ANG stimulates VEGF receptor signaling and downstream effectors of insulin signaling. (**a**) Western blot analyses depicting enhanced expression of pVEGFR2 and its downstream member pSrc as well as the pRPS6 that triggers ribosomal biogenesis in HUVECs in the presence of increasing concentrations (0, 250, 500, 1,000 ng/ml) of rhANG for 6 hours. (**b**) Densitometric analysis of western blots depicted in Supplementary Figure S5a. (**c**) Quantification of ANG-positive cells in sections from biopsies of human AWs, chronic DWs, and CVUs shown in Figure 4e. Statistical analysis was performed using one-way ANOVA; values are represented as mean ± SEM, n = 3. ANG, angiogenin; AW, acute wound; CVU, chronic venous leg ulcer; DW, diabetic wound; HUVEC, human umbilical vein endothelial cell; pRPS3, phosphorylated RPS6; pSrc, phosphorylated Src; pVEGFR2, phosphorylated VEGF receptor 2; rh, recombinant human.
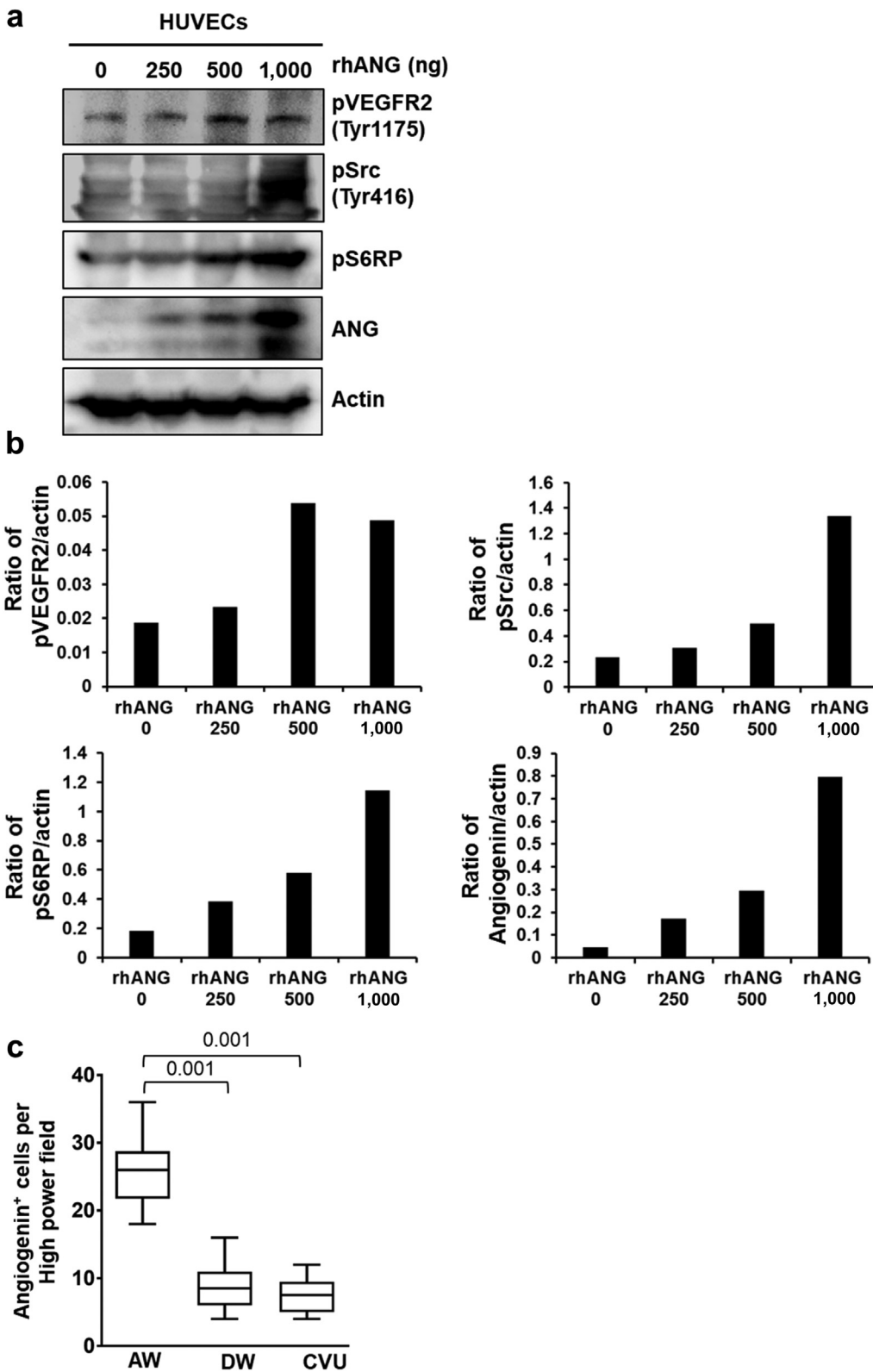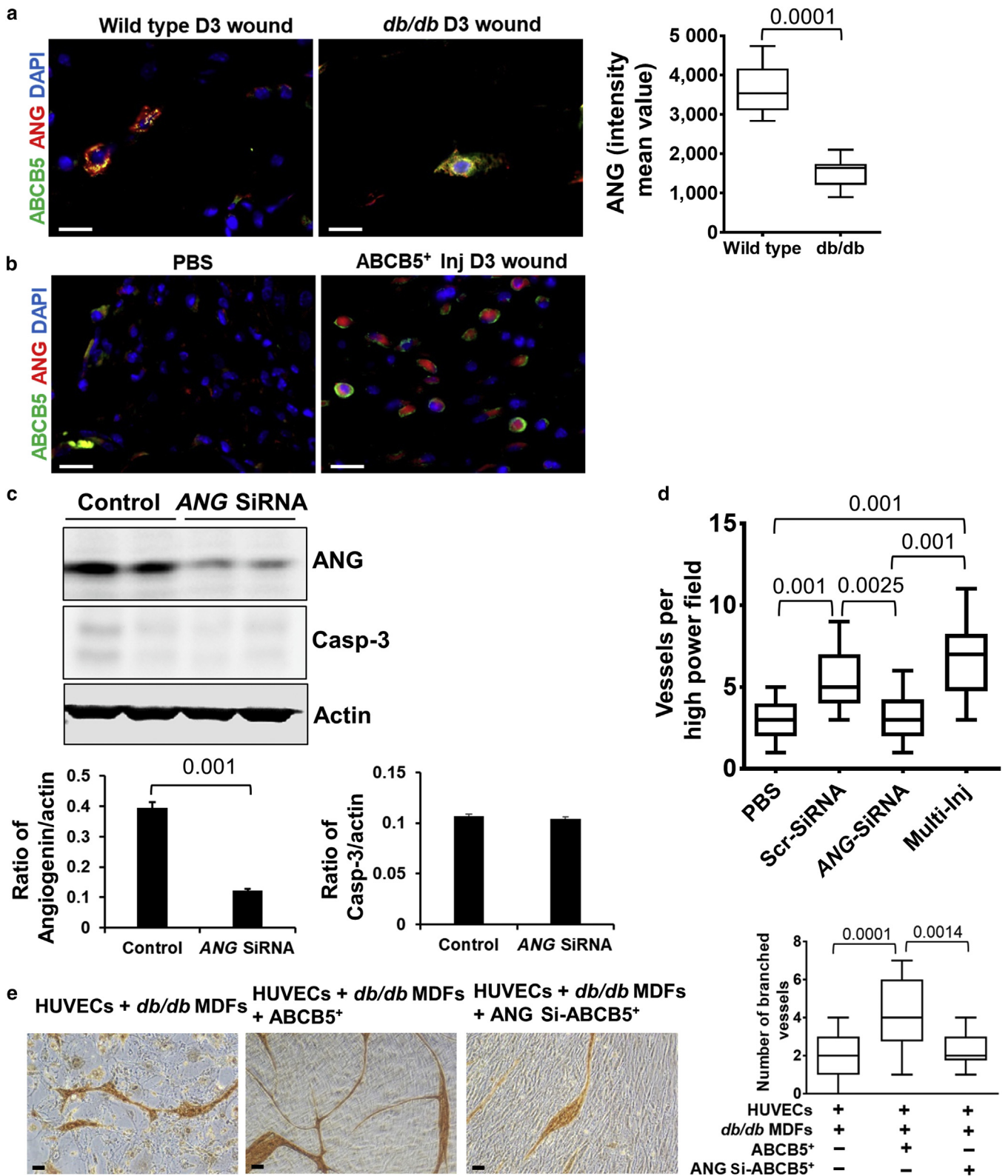
Supplementary Figure S6. Diabetic microenvironment suppresses angiogenesis. (**a**) Immunostaining and quantification of ANG (red) in ABCB5^{+} precursors (green) in D3 wounds of wild-type mice and mice with diabetes. Statistical analysis was performed using unpaired *t*-test (mean ± SEM), n = 3. Bar = 20 μm. (**b**) Immunostaining of ANG (red) and ABCB5 (green) marking human ABCB5^{+} SPs in wounds aged 3 days injected either with PBS or human ABCB5^{+} SPs. Bar = 20 μm, n = 3. (**c**) Western blot analysis depicting the expression of ANG and the cleaved caspase-3, indicative of apoptosis in scr or ANGSi-ABCB5^{+} SPs. (**d**) Quantification of blood vessels depicted in Figure 5c. Quantitative analysis is performed in images captured with ×40 objective. Statistical analysis was performed using one-way ANOVA (mean ± SEM), n = 3. (**e**) In vitro angiogenesis and its quantification from the indicated groups. Bar = 50 μM. Statistical analysis was performed using one-way ANOVA (mean ± SEM), n = 3. ANG, angiogenin; ANGSi-ABCB5^{+}, angiogenin-silenced ABCB5^{+} SP; D, day; HUVEC, human umbilical vein endothelial cell; inj, injections; MDF, murine dermal fibroblast; scr, scrambled; siRNA, small interfering RNA; SP, stromal precursor.
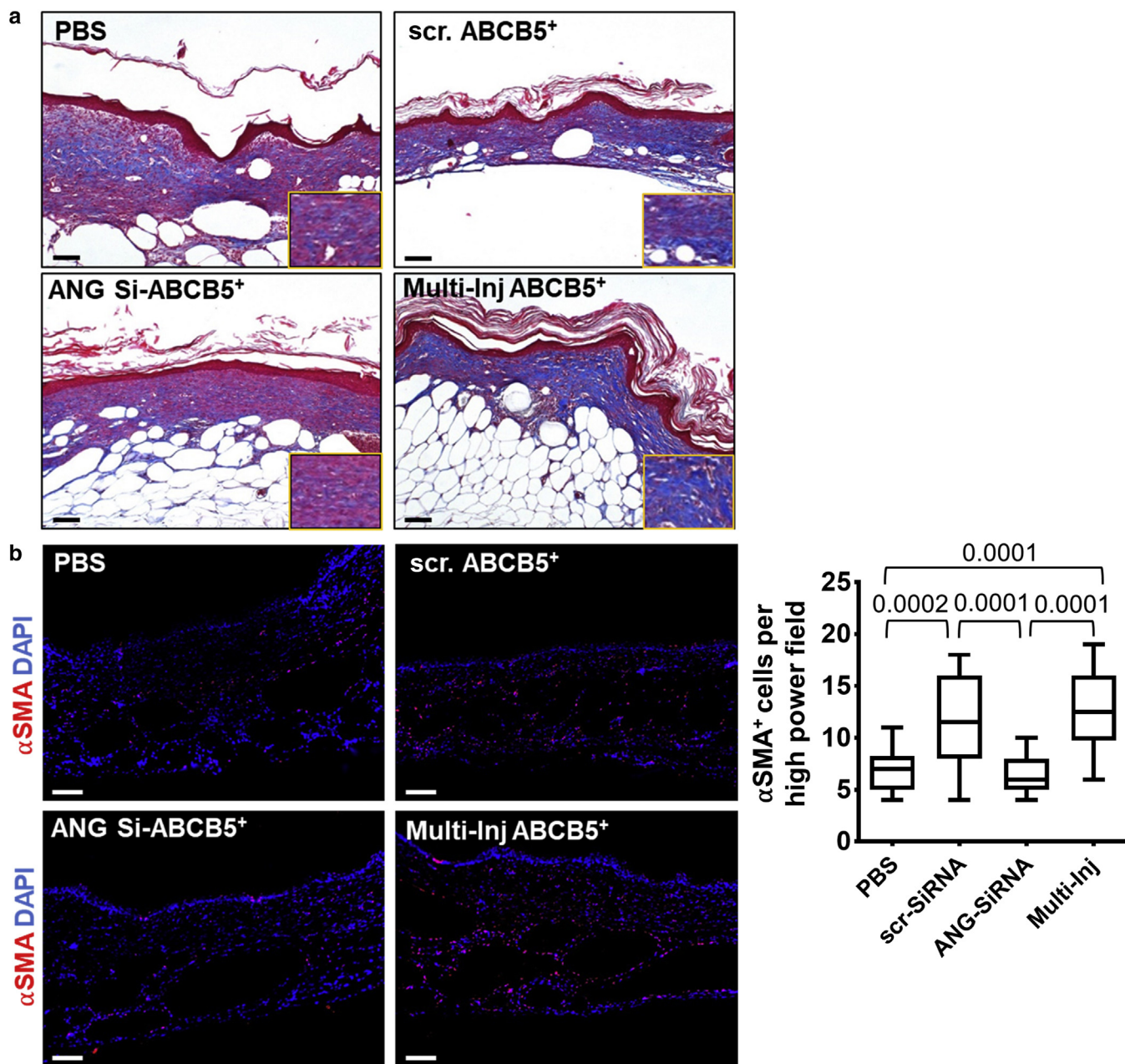
Supplementary Figure S7. ANG plays a critical role in ABCB5$^+$ SPs–mediated wound remodeling. (**a**) Masson's trichrome staining visualizing the thickness and organization of dermal collagen fibrils (blue) after injection of PBS (vehicle control), scr ABCB5$^+$ SPs, or ANG-silenced ABCB5$^+$ SPs or after repetitive injections of ABCB5$^+$ SPs into *db/db* mice wounds. Bar = 100 μm. (**b**) Immunostaining and quantification of the myofibroblasts-specific marker α-SMA (red) after injection of PBS (vehicle control), scr ABCB5$^+$ SPs, and ANG-silenced ABCB5$^+$ SPs or after repetitive injections of ABCB5$^+$ SPs into *db/db* mice wounds. Quantitative analysis is performed in images captured with ×40 objective. Nuclei were stained with DAPI (blue). Bar = 100 μm. Statistical analysis was performed using one-way ANOVA; values are represented as mean ± SEM, n = 3. αSMA, α-smooth muscle actin; ANG, angiogenin; Scr, scrambled; siRNA, small interfering RNA; SP, stromal precursor.

Supplementary Table S1. Demographic and Other Key Characteristics of the Patients

Sample	Age	Gender (M/F)	Ethnicity (AA/H/HW/W)	HbA1c
DFU	63	M	W	6.5
DFU	59	M	HW	6.0
DFU	67	F	AA	9.8
DFU	53	M	H	8.5
CVU	76	M	W	—
CVU	69	F	W	—
CVU	71	M	W	—
AW	23	M	W	—
AW	22	F	W	—
AW	25	F	W	—

Abbreviations: AA, African American; AW, acute wound; CVU, chronic venous leg ulcer; DFU, diabetic foot ulcer; F, female; H, Hispanic; HbA1c, hemoglobin A1c; HW, Hispanic White; M, male; W, White.